

Supplementary Information

X-ray crystallographic analysis of the antiferromagnetic low-temperature phase of galvinoxyl: Investigating magnetic duality in organic radicals

Rie Suizu, Yoshiaki Shuku, Vincent Robert, Pablo Roseiro, Nadia Ben Amor, Zain Khawar, Neil Robertson, and Kunio Awaga

1. Magnetic susceptibility

Magnetic susceptibility measurements for galvinoxyl were conducted on polycrystalline samples using an MPMS-XL Quantum Design magnetometer, to confirm the presence of the phase transition and the high sample purity. A plastic straw was employed as the sample holder during the measurements. The measurements were carried out at temperatures ranging from 2 to 300 K under a magnetic field of 0.5 T. To determine the temperature dependence of the paramagnetic susceptibility χ_p , the experimentally obtained diamagnetic susceptibility χ_{dia} of $-5.31 \times 10^{-4} \text{ cm}^3 \text{ mol}^{-1}$ was utilized, assuming that χ_p follows the Curie-Weiss law (eq. 1) in the high-temperature phase.

$$\chi_M = \chi_p + \chi_{dia} = \frac{C}{T - \theta} + \chi_{dia}$$

The results are shown in Fig. S1, where the green curves indicate the theoretical best fit of the Curie-Weiss law in temperature range of 86-300 K with the Curie constant C of $0.374 \text{ cm}^3 \text{ mol}^{-1} \text{ K}$ and the Weiss constant θ of 12.2 K for the HT phase.

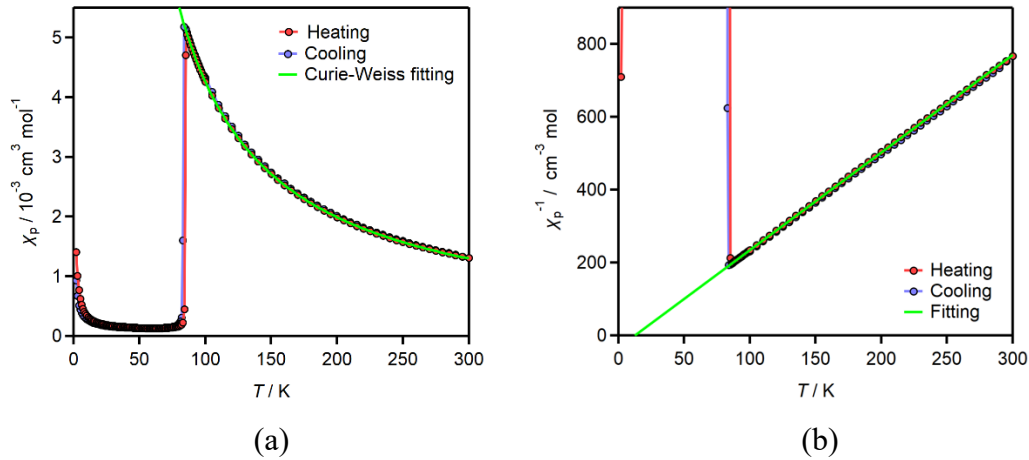


Figure S1. Temperature dependence of χ_p (a) and χ_p^{-1} (b) for galvinoxyl, prepared in this study.

2. Crystal structure analysis

The X-ray diffraction data for single crystal structure analysis were collected on a Rigaku AFC-10 instrument equipped with a MicroMax-007 microfocus rotating anode X-ray generator by using graphite-monochromated Mo K α radiation ($\lambda = 0.71073 \text{ \AA}$) and a HyPix6000 hybrid photon counting detector under a cold nitrogen stream installed in Chemical Instrumentation Facility, Research Center for Materials Science, Nagoya University for the high temperature phase, and under a cold helium stream installed in Instrument Center of Institute for Molecular Science, Japan for the low temperature phase. The frame data were integrated and corrected for absorption with the Rigaku Oxford Diffraction CrysAlisPro package.^{S1} The crystal structure was solved using intrinsic phasing methods (SHELXT-2018/2)^{S2} and standard difference map techniques and refined by full-matrix least-square procedures on F^2 (SHELXL-2018/3).^{S3} All non-hydrogen atoms were refined anisotropically. All hydrogen atoms were placed at calculated positions and refined using a riding model. All calculations were performed using the OlexSys Olex2 crystallographic software package.^{S4} Details of the crystal data and a summary of the intensity data collection parameters of X-ray crystallography are listed in Table S1, and the selected bond lengths and angles are summarized in Table S2.

Table S1. Crystallographic Data for galvinoxyl radical.

	HT phase	LT phase ^c
formula		C ₂₉ H ₄₁ O ₂
fw		421.62
<i>T</i> (K)	123(2)	50(2)
λ (Å)		0.71073
cryst system	monoclinic	triclinic
space group	<i>I</i> 2/a (#15)	<i>P</i> -1 (#2)
<i>a</i> (Å)	10.5123(3)	10.3090(15)
<i>b</i> (Å)	10.6991(3)	12.8561(13)
<i>c</i> (Å)	22.8903(7)	20.165(2)
α (degree)	90	77.953(9)
β (degree)	99.837(3)	81.876(11)
γ (degree)	90	74.138(11)
<i>V</i> (Å ³)	2536.67(13)	2504.0(6)
<i>Z</i>	4	4
<i>D</i> _{calc} (g / cm ³)	1.104	1.118
μ (mm ⁻¹)	0.067	0.068
<i>F</i> (000)	924	924
cryst size (mm)	0.3 × 0.06 × 0.04	0.30 × 0.10 × 0.03
θ range (deg)	3.312–29.129	2.062–29.925
reflns collected	19035	27511
indep reflns/ <i>R</i> _{int}	3364/ 0.0306	27511 / 0.154
params	147	584
GOF on <i>F</i> ²	1.058	0.930
<i>R</i> ₁ ^a , <i>wR</i> ₂ ^b [<i>I</i> > 2 σ (<i>I</i>)]	0.0463, 0.1289	0.1160, 0.2111
<i>R</i> ₁ ^a , <i>wR</i> ₂ ^b (all data)	0.0516, 0.1333	0.2909, 0.3362

$$^a R_1 = \Sigma ||F_o| - |F_c|| / \Sigma |F_o|. \quad ^b wR_2 = [\Sigma \{w(F_o^2 - F_c^2)^2\} / \Sigma w(F_o^2)^2]^{1/2}.$$

$$^c S = [\Sigma \{w(F_o^2 - F_c^2)^2\} / (N_{\text{ref}} - N_{\text{par}})]^{1/2}$$

^c Two components twin (BASF 0.4017(19))

Table S2. Selected bond lengths and angles

	HT phase	LT phase	
		A	B
Intramolecular bond lengths			
O1-C1	1.2341(13)	1.253(6)	1.243(6)
O2-C13		1.237(6)	1.244(6)
C1-C2	1.4860(13)	1.463(8)	1.466(8)
C1-C3	1.4812(13)	1.488(8)	1.497(7)
C2-C4	1.3606(13)	1.362(7)	1.369(7)
C3-C5	1.3578(13)	1.367(7)	1.366(7)
C4-C6	1.4332(13)	1.434(7)	1.430(7)
C5-C6	1.4340(12)	1.424(8)	1.425(8)
C6-C7	1.4067(10)	1.416(7)	1.408(7)
C7-C8		1.406(7)	1.403(7)
C8-C9		1.437(8)	1.437(8)
C8-C10		1.426(8)	1.428(8)
C9-C11		1.365(7)	1.360(7)
C10-C12		1.369(7)	1.362(7)
C11-C13		1.478(8)	1.479(8)
C12-C13		1.486(8)	1.477(7)
Intramolecular angles			
C6-C7-C6 ^a	132.98(12)		
C6-C7-C8		133.3(6)	130.7(6)
Intermolecular bond lengths			
C6-C6 ^b	3.903		
C6A-C6B		3.249	
C8A-C8B ^c		4.464	

^a1/2-x, y, 1-z, ^b1-x, 1-y, 1-z, ^c-1+x, y, z

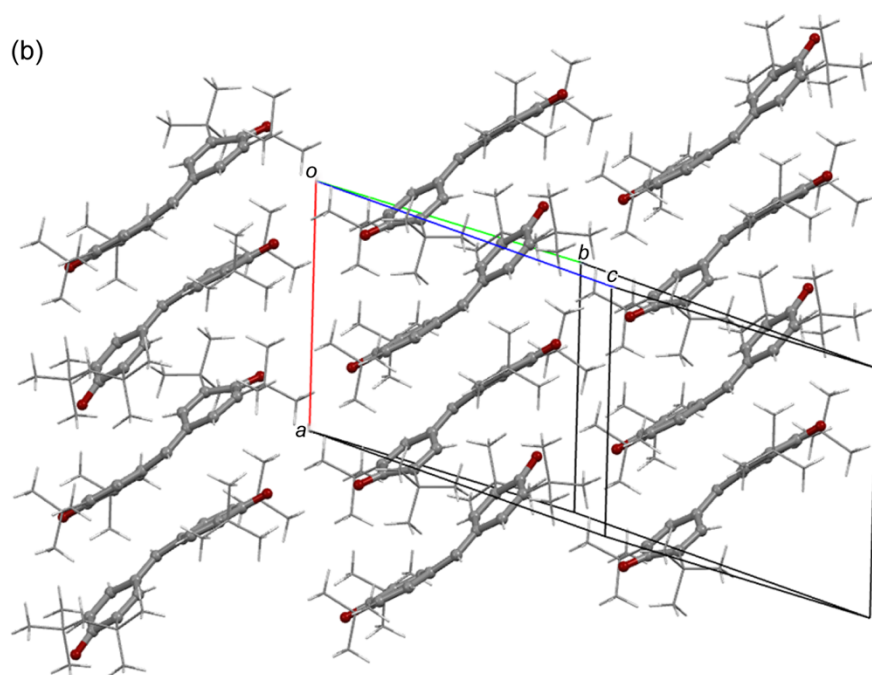
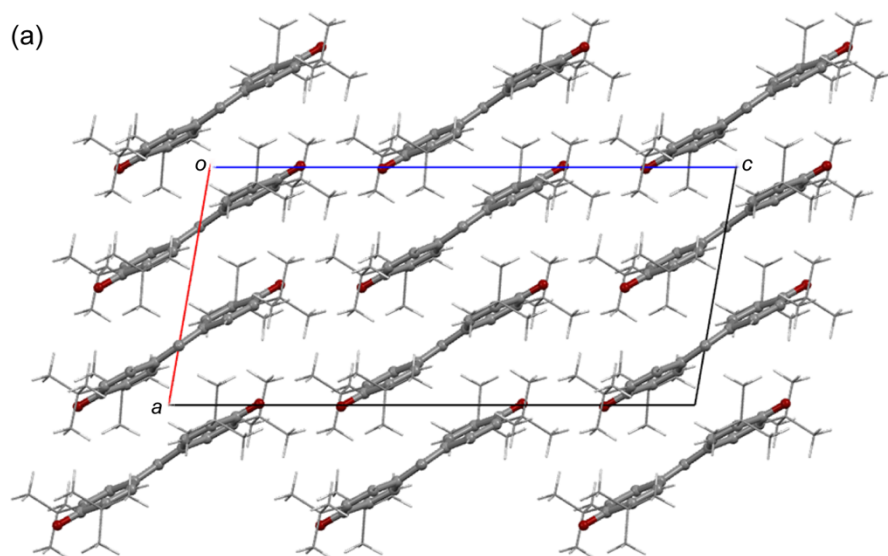
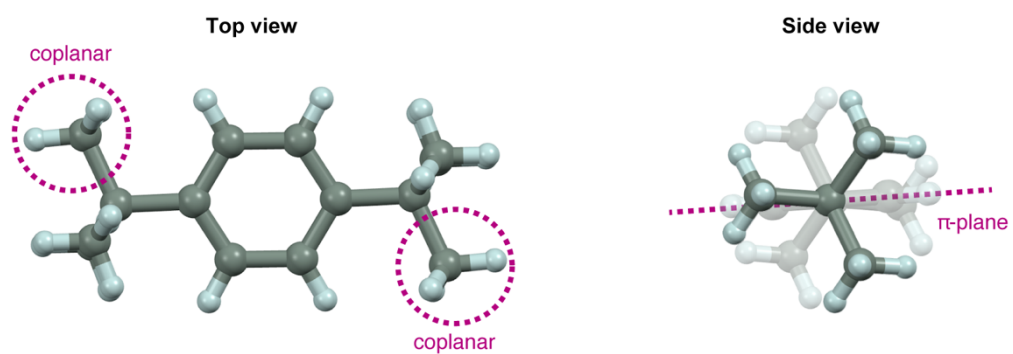


Figure S2. Molecular arrangements in HT phase (a) and LT phase (b).

(a) 1,4-Di-*t*-butylbenzene (BUTBNZ01: CCDC 869185)



(b) 1,3,5-Tri-*t*-butylbenzene (TTBUBZ01: CCDC 1525484)

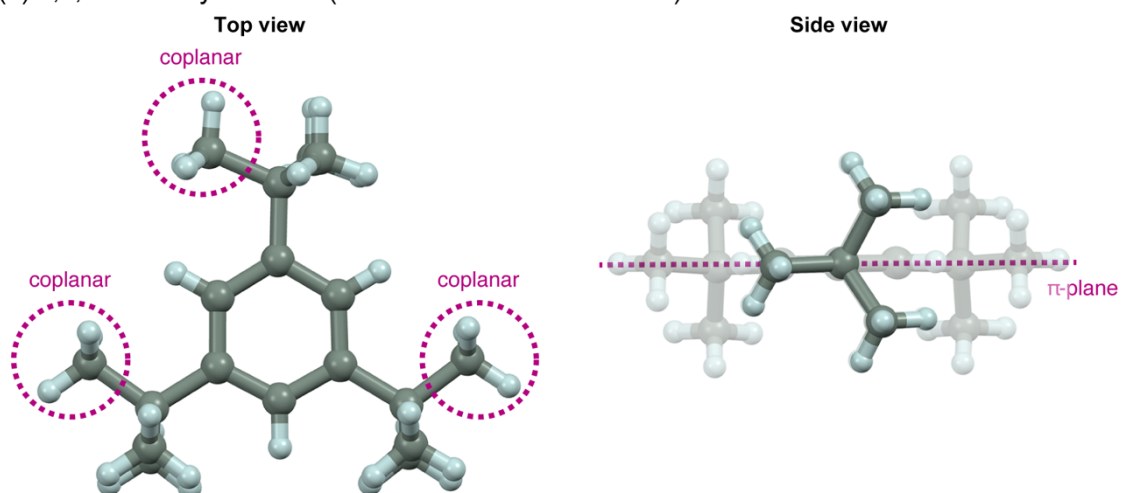


Figure S3. Molecular structures of di- and tri-substituted *t*-butylbenzenes.^{S5,6}

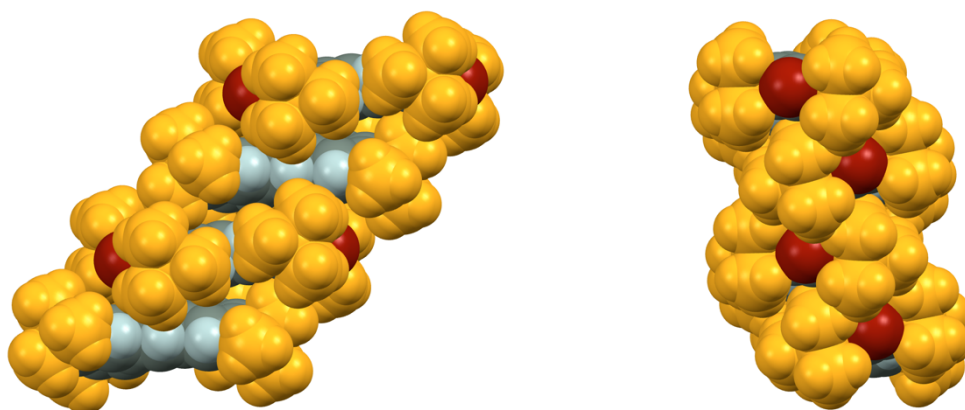


Figure S4. Steric effects of the bulky *t*-butyl groups.

3. Theoretical consideration using allyl radical

The magneto-structural correlations of galvinoxyl in the HT and LT phases can qualitatively be explained using a model compound, the allyl radical. It is known that the node of the SOMO of this molecule appears on the central carbon, and its anti-nodes of different phases appear on the terminal carbons (See Fig. S4). Figure S5 shows two types of intermolecular overlap for the allyl radical, namely Type-A and Type-B. In the Type-A arrangement, the node and anti-node carbons are facing each other, so that two SOMOs are nearly orthogonal. Therefore, we can expect a FM intermolecular interaction following Hund's rule. In contrast, the Type-B arrangement includes a short distance between the anti-node carbons, indicating a significant overlap between the SOMOs. This should result in a strong AFM coupling. The present structural analysis concludes that the intermolecular arrangement of galvinoxyl in the HT and LT phases corresponds to Type-A and Type-B arrangements, respectively.

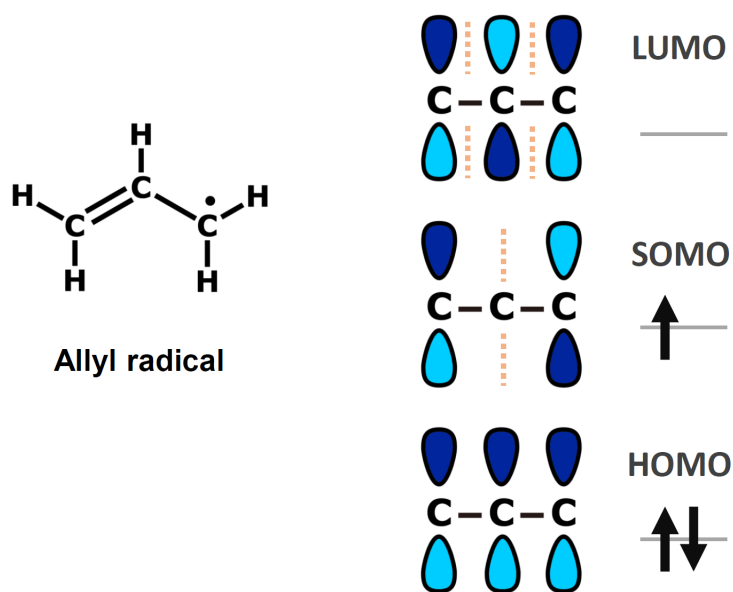


Figure S5. Molecular orbitals of allyl radical.

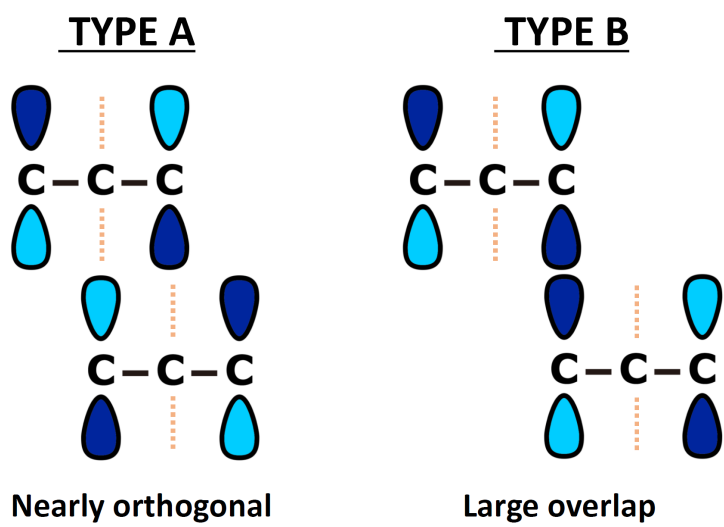


Figure S6. Two kinds of intermolecular overlaps of allyl radical.

4. Theoretical calculations

To get a better insight into the LT and HT magnetic behaviors, quantum chemistry calculations were carried out on pairs of radicals, assuming the Hamiltonian, $H = -2J \mathbf{S}_1 \cdot \mathbf{S}_2$. The presence of multiple open-shells invites the use of a wavefunction-based method, such as the complete active space self-consistent field (CASSCF) method. To reduce the computational time, the four *t*-butyl groups of the galvinoxyl radical were substituted by methyl groups without any further geometry optimization by fixing the C-C and C-H bond distances to 1.54 and 1.09 Å, respectively. The minimal active space includes two electrons in two orbitals to generate CAS[2,2] molecular orbitals (MOs). All CASSCF calculations were performed on the simplified LT and HT X-ray structures using the MolCAS 7.8.^{S7} The methyl groups were described with small basis sets (i.e., 2s1p and 2s for C and H atoms, respectively). More extended basis sets 3s2p1d were used for all other C and O atoms. The dynamical correlation and polarization effects were included following the Difference Dedicated Configuration Interaction (DDCI) method^{S8,S9} as implemented in the CASDI code.^{S9} This variational method that follows a step-by-step construction of the wavefunction has produced a wealth of interpretations and rationalizations in particular in the field of molecular magnetism involving organic radical ligands.^{S10-12} The methodology relies on the construction of wavefunctions on the basis of a unique MOs basis set. Depending on the class of determinants involved in the CI expansion, one gives rise to CAS+S and CAS+DDCI3 singlet-triplet $\Delta_{ST} = E(S=0) - E(S=1)$ energy differences in the LT and HT phases. Based on the triplet MOs generated from CAS[2,2]SCF calculations in the LT and the HT phases, CAS+S and CAS+DDCI3 calculations allowed us to identify the nature of the magnetic interactions and evaluate their amplitudes. As summarized in Table S3, the nature of the interaction changes from strong antiferromagnetic (LT) to weak ferromagnetic (HT) along the transition. Our calculations confirm the significant modifications of the magnetic behavior upon heating.

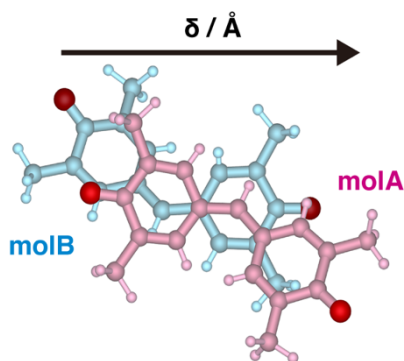
Table S3. Singlet-triplet Δ_{ST} (in K) energy differences calculated at CAS[2,2]+S and CAS[2,2]+DDCI3 levels for the simplified dimers extracted from the LT and HT phases.

Δ_{ST} / K	CAS+S	CAS+DDCI3
LT phase	-822	-1069
HT phase	31	36

We computed Δ_{ST} for hypothetical dimer structures, wherein one molecule of the dimer in the LT phase was incrementally shifted in parallel (see the inset in Table S4). To reduce the computational cost of this qualitative inspection, calculations were performed at the CAS+DDCI2 level. The results are shown in Table S4, where the structure at $\delta = 0 \text{ \AA}$ represents the LT phase. For this particular structure, the computed Δ_{ST} value changes by less than 6% between CAS+DDCI2 (Table S4) and CAS+DDCI3 (Table S3). Let us stress that Δ_{ST} is not affected by slippages along the perpendicular direction.

Table S4. Singlet-triplet Δ_{ST} (in K) energy differences calculated at CAS[2,2]+DDCI2 level for hypothetical dimer structures. The inset shows the geometry for the calculation, where the molecule A (magenta) of the dimer was incrementally shifted in parallel along the arrow direction.

$\delta / \text{\AA}$	0	0.185	0.370	0.555
$\Delta_{\text{ST}} / \text{K}$	-1015	-743	-455	-54



REFERENCES

- [S1] CrysAlisPro 1.171.40.67a, (Rigaku Oxford Diffraction, 2019).
- [S2] G. M. Sheldrick, SHELXT – Integrated space-group and crystal-structure determination. *Acta Cryst.*, 2015, **A71**, 3-8.
- [S3] G. M. Sheldrick, Crystal structure refinement with SHELXL. *Acta Cryst.*, 2015, **C71**, 3-8.
- [S4] Olex2 1.5, O. V. Dolomanov, L. J. Bourhis, R. J. Gildea, J. A. K. Howard, H. Puschmann, OLEX2: a complete structure solution, refinement and analysis program. *J. Appl. Cryst.*, 2009, **42**, 339-341.
- [S5] M. F. Ibad, P. Langer, A. Schulz, A. Villinger, *J. Am. Chem. Soc.*, 2011, **133**, 21016-21027.
- [S6] P. Beckmann, A. L. Rheingold, *CSD Communication* (2018).
- [S7] F. Aquilante, J. Autschbach, R. K. Carlson, L. F. Chibotaru, M. G. Delcey, L. de Vico, I. F. Galván, N. Ferré, L. M. Frutos, L. Gagliardi, M. Garavelli, A. Giussani, C. E. Hoyer, G. L. Manni, H. Lischka, D. Ma, P. Å. Malmqvist, T. Müller, A. Nenov, M. Olivucci, T. B. Pedersen, D. Peng, F. Plasser, B. Pritchard, M. Reiher, I. Rivalta, I. Schapiro, J. Segarra-Martí, M. Stenrup, D. G. Truhlar, L. Ungur, A. Valentini, S. Vancoillie, V. Veryazov, V. P. Vysotskiy, O. Weingart, F. Zapata, R. Lindh, Molcas 8: New capabilities for multiconfigurational quantum chemical calculations across the periodic table. *J. Comput. Chem.*, 2016, **37**, 506-541.
- [S8] J. Miralles, O. Castell, R. Caballol, J.-P. Malrieu, Specific CI calculation of energy differences: Transition energies and bond energies. *Chem. Phys.*, 1993, **172**, 33-43.
- [S9] N. Ben Amor, D. Maynau, Size-consistent self-consistent configuration interaction from a complete active space. *Chem. Phys. Lett.*, 1998, **286**, 211–220.
- [S10] L. Norel, J.-B. Rota, L.-M. Chamoreau, G. Pilet, V. Robert, C. Train, Spin Transition and Exchange Interaction : Janus Visions of Supramolecular Spin Coupling Between Face-to-Face Verdazyl Radicals *Angew. Chem. Int. Ed.*, 2011, **123**, 7266-7269.
- [S11] Y. Shuku, R. Suizu, A. Domingo, C. J. Calzado, V. Robert, K. Awaga, Multidimensional Network Structures and Versatile Magnetic Properties of Intermolecular Compounds of a Radical–Anion Ligand, [1,2,5]Thiadiazolo[3,4-*f*][1,10]phenanthroline 1,1-Dioxide. *Inorg. Chem.*, 2013, **52**, 9921-9930.
- [S12] A. Domingo, M. Vérot, F. Mota, C. de Graaf, J. J. Novoa, V. Robert, Impact of Short and Long-Range Effects on the Magnetic Interactions in Neutral Organic Radical-Based Materials. *Phys.Chem. Chem.Phys.*, 2013, **15**, 6982-6989.